The Utilization of Nimbus-7 SMMR Measurements to Delineate Rainfall over Land

EDWARD RODGERS

Laboratory for Atmospheric Sciences, Goddard Space Flight Center/NASA, Greenbelt, MD 20771

HONNAPPA SIDDALINGAIAH

OAO Corporation, Greenbelt, MD 20770

(Manuscript received 2 September 1982, in final form 11 April 1983)

ABSTRACT

In light of previous theoretical calculations, an empirical-statistical analysis using satellite multifrequency dual polarized passive microwave data to detect rainfall areas over land was performed. The addition of information from a lower frequency channel (18.0 or 10.7 GHz) was shown to improve the discrimination of rain from wet ground achieved by using a single frequency dual polarized (37 GHz) channel alone.

The algorithm was developed and independently tested using data from the Nimbus-7 Scanning Multichannel Microwave Radiometer (SMMR). Horizontally and vertically polarized brightness temperature pairs (T_H, T_V) at 37, 18, 10.7 GHz were sampled for rain areas over land (determined from ground-based radar), wet ground areas (adjacent and upwind from rain areas determined from radar), and dry land regions (areas where rain had not fallen during a previous 24 h period) over the central and eastern United States. Surface thermodynamic temperatures were both above and below 15°C. An examination of the data from each separate channel indicated that the probability (using the F test) for the mean vectors of any two populations being identical is less than 0.01 for classes sampled with surface thermodynamic temperatures $\geq$15°C except for the rain over land and wet ground classes observed with the SMMR 37 GHz channel. For the classes sampled with surface thermodynamic temperatures < 15°C, none of the classes were significantly different.

Since most of the categories were significantly different for the warmer ($\geq$15°C) land surface cases, a Fisher linear discriminant classifier was then developed for each channel and independently tested. The results from one test case showed that for areas of large-scale heavy rainfall, the lower frequency SMMR channels were better able to delineate rain from wet ground than the 37 GHz channel. However, in areas of light rain and/or where the rain area did not fill the lower frequency instantaneous field of view these channels were not able to differentiate rain from wet ground.

1. Introduction

Theoretical calculations (Savage and Weinman, 1975; Savage *et al.*, 1976; and Wienman and Guetter, 1977) have indicated that at 37 GHz rainfall could be detected over land surfaces. These results showed that at 37 GHz and at a viewing angle of 50° from nadir the radiance emerging from hydrometers is relatively small (due to scattering) and unpolarized, whereas radiance emerging from wet land surfaces is also relatively small but polarized, and radiance emerging from dry land surfaces is relatively large. These results were partially verified empirically by Rodgers *et al.* (1979) by studying large scale rainfall over land utilizing the Nimbus-6 Electrically Scanning Microwave Radiometer (ESMR-6) data. The study showed that a large scale rainfall over land, where surface thermodynamic temperatures were greater than 15°C, and where the vegetation was not covered with dew could be delineated from dry land surfaces despite the large ESMR-6 instantaneous field of view (IFOV). However, the delineation of rain from wet land surfaces was found to be more difficult.

For the purpose of developing an improved passive microwave technique to delineate rain from wet land surfaces, results from a radiative transfer model suggested using dual polarized multifrequency passive microwave data where the 37 GHz frequency channel data would be augmented by data from the lower frequency channels at 18.0 and 10.7 GHz. These lower frequency channels should have a better capability to differentiate rainfall from land surfaces. This is demonstrated in Fig. 1, which displays the theoretically calculated dual polarized 37.0, 18.0, and 10.7 GHz brightness temperatures (T_B) at 50° incidence angle with the earth surface for a given rain rate. These T_B's were derived from a radiative transfer model with Lambertian reflection (Born and Wolf, 1975) from land surfaces at a thermodynamic temperature of 299.1 K and with a fixed dielectric constant that simulates wet soil of 20% soil moisture content (i.e., a wet ground case) and an atmospheric freezing level at 4 km (Wilheit *et al.*, 1977).

There are several features of interest that Fig. 1 delineates. First, the difference between the vertically polarized $T_B(T_V)$ and the horizontally polarized

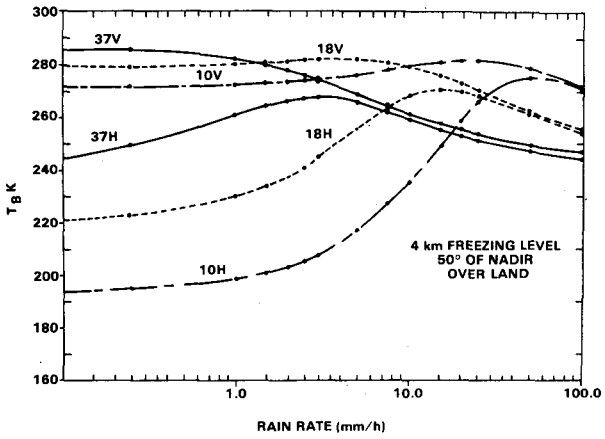

FIG. 1. Computed horizontally and vertically polarized brightness temperatures at 37.0, 18.0 and 10.7 GHz as a function of rain rate.

$T_B(T_H)$ decreases with increasing rain rates; second, the higher the frequency, the more sensitive T_H is to rain (e.g., the highest frequency T_Bs are affected more by the absorption and re-emission and scattering of radiation from rain drops); third, the lower the frequency, the colder the T_B for wet land surfaces with minimum rain rates; fourth, absorption and re-emission of radiation from raindrops affects the T_H more than T_V, and finally, the lower the frequency, the larger the net warming of T_H over the displayed range of rain rates.

To differentiate rain from wet land surface using the dual polarized 37 GHz T_B's measured from ESMR-6, Rodgers *et al.* (1979) relied on the fact that as the rain rate increased, the strong backscattering by the larger raindrops decreased the polarization difference. However, as delineated by Fig. 1 the change in the 37 GHz T_V and T_H channel curves are small for increasing rain rates. The small dynamic range in T_B for increasing rain rates, together with the large ESMR-6 IFOV were the major contributing factors leading to the difficulties in differentiating rain from wet land surfaces. Since rain that was observed with ESMR-6 sometimes did not fill the sensors IFOV, the sensor was observing the partially wet land surface background causing T_Bs to be cooler and more polarized than if the sensor's IFOV was completely filled with rain. These T_Bs were comparable to the surrounding nonraining wet land surfaces T_B because of the small dynamic range in T_B for increasing rain rates. To eliminate this problem, the theoretical model suggests that data from the lower frequency channels with their larger dynamic range in T_H should be used to augment the 37 GHz frequency data. If rain rates are large enough so that radiance emitted from the rain drops is sufficient to warm significantly the 18.0 and 10.7 GHz T_H above the nonraining wet land surface background T_H, the lower frequencies will improve the delineation of rain from wet land surfaces.

It is the purpose of this work to study the application of these ideas with empirical data for the purpose of recommending an improved satellite technique for delineation of rain over land. This will be accomplished by statistically analyzing the Nimbus-7 *S*canning *M*ultichannel *M*icrowave *R*adiometer (SMMR) 37.0, 18.0 and 10.7 GHz data. This statistical analysis will be performed on each channel first by sampling the T_B's of the three SMMR channels, together with the GOES-1 Visible Infrared Spin Scan Radiometer (VISSR) infrared (11 μm) data for three categories of SMMR T_B's representing rainfall over land, wet land surface without rain, and dry land surfaces and then by testing these populations for uniqueness and separability. A Fisher (1938) linear discriminant classifier will be developed for each SMMR channel and the performance of these algorithms will be checked using an error estimate and with an independent test case. Finally, after considering the results of this study, recommendations will be made concerning a satellite technique that utilizes infrared and dual polarized multifrequency passive microwave data to detect rainfall over land with improved accuracy.

2. The SMMR system

The SMMR flown aboard Nimbus-7 (Gloerson and Hardis, 1978) which was launched in 1978, measures thermal radiation upwelling from the earth's surface and the intervening atmosphere at 5 frequencies, 37.0, 18.0, 21.0, 10.7, and 6.6 GHz. The antenna scans mechanically ±25° in azimuth every 4 s along a conical surface with a vertical axis and a 42° cone angle making a constant incidence angle with the earth's surface of 50°. The instrument measures both horizontal and vertical polarization components for all frequencies. At the four lower frequencies, the radiometers are time-shared between the two polarizations, while at 37.0 GHz there are two radiometers, one for each polarization. Because the radiometers for lower frequencies of SMMR are time-shared by the vertical and horizontal polarization components, the two polarizations are not viewed simultaneously, causing a maximum offset of approximately 28 km between IFOVs with respect to the earth's surface. For the 37.0 GHz channel, the two polarizations are viewed simultaneously. When sampling the lower SMMR frequencies in this study, no attempt was made to correct for this misalignment. The IFOV of the instrument, being proportional to wavelength, ranges from ~150 km at 6.6 GHz to 30 km at 37.0 GHz. The data are calibrated using a warm (instrument ambient) and cold (cosmic background) input to the radiometer. The instrument is described in more detail by Gloersen and Barath (1977).

3. Data sampling

Simultaneous radar measurements of rain and SMMR 37.0, 18.0 and 10.7 GHz T_Bs were needed to sample a given SMMR channel IFOV as rainfall over land, dry land surfaces, or wet land surfaces. Six daytime synoptic-scale rainfall cases over the eastern and central United States were used where rain data taken from the National Weather Service's WSR-57 radars coincided with the SMMR overpass to within 5 min. In two of the cases, the surface thermodynamic temperatures were $\geq 15°C$, while in the other cases, the thermodynamic temperatures were $<15°C$. The cases with the warm surface background had moderate to heavy rain associated with a squall line (30 May 1979) and hurricane David (3 September 1979). Sampling for this study was performed under the following conditions: 1) rain areas were defined as regions where rain rates were ≥ 2.5 mm h^{-1} as delineated by the WSR-5 radar; 2) wet land surfaces were defined as regions not raining but had rained in the past hour and usually located upwind and adjacent to the rain cells observed on the WSR-57 radar; and 3) dry land surfaces were defined as regions where rain had not fallen within a 24 h period previous to the Nimbus-7 pass as determined by surface synoptic maps. The six cases are given in Table 1.

In order to sample the SMMR data, NASA's Atmospheric and Oceanographic Information Processing System (AOIPS) was used to overlay the SMMR and the WSR-7 radar PPI images upon the GOES-1 infrared digital images. A remapping was performed using bilinear interpolation with nearest neighbor resampling and then the AOIPS was used to sample the SMMR data.

An example of the products derived from the remapping program on AOIPS are seen in Figs. 2–4. Figs. 2, 3, and 4 are, respectively, the GOES-1 infrared image; the PPI image from the Lake Charles, Louisiana, WSR-57 radar; and the SMMR vertically polarized 37.0 GHz image of a squall line over the Oklahoma, Texas and Louisiana area at 1743 GMT on 30 May 1979. The GOES-1, SMMR, and WSR-57 radar data were taken within 5 min of each other. In the radar image, the lightest shades represent rain rates > 2.5 mm h^{-1}. The infrared image has been enhanced to help delineate the most active convection. Cloud tops were shaded into four grey scales (black-to-white stepped every 64 grey scales) corresponding to equivalent blackbody temperatures (T_{BB}) of 270–240 K, 239–220 K, 219–210 K, and ≤ 209 K, respectively. Clouds with $T_{BB} \leq 270$ K are probably producing rain (Shenk *et al.*, 1976) and those with $T_{BB} < 209$ K are probably producing convective rain (Negri and Adler, 1981). In the SMMR 37 GHz image, the light (dark) shades represent the warmer (colder) T_B. The T_B values from all the SMMR channels are a function of radiance emerging from the earth's surface and the state of the intervening atmosphere. The microwave radiance emitted from the earth's surface is given by ϵT_s, where ϵ is the surface

TABLE 1. Rain cases.

Case	Date (1979)	Time (GMT)
1	20 April	1730
2	2 May	1630
3	4 May	1730
4	30 May	1743
5	3 September	1615
6	5 October	1630

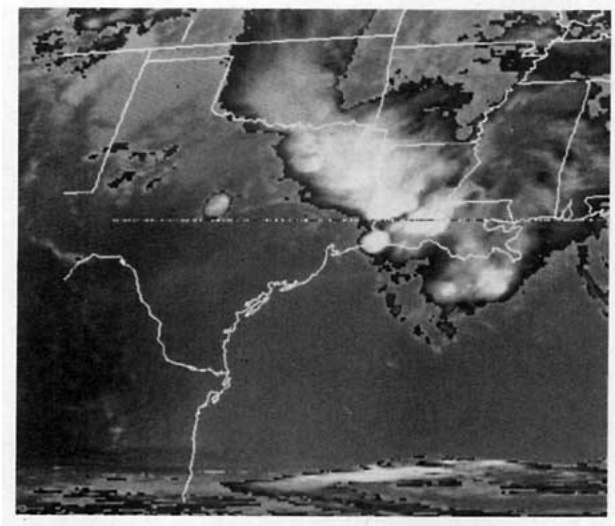

FIG. 2. The GOES-1 infrared image of a squall line observed at 1743 GMT on 30 May 1979. (See text.)

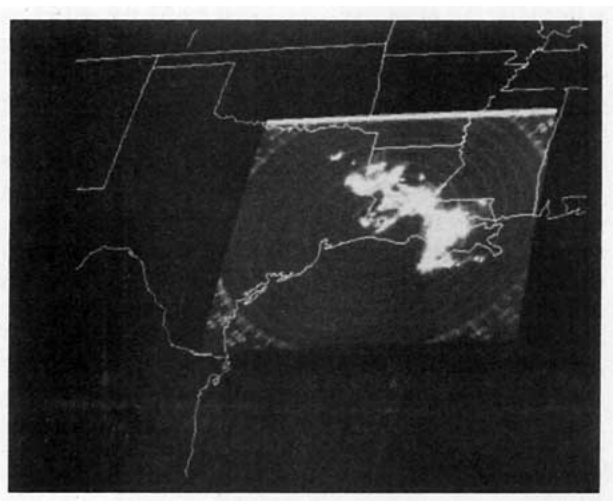

FIG. 3. The PPI image from the Lake Charles, Louisiana, WSR-57 radar at 1743 GMT on 30 May 1979. Bright areas represent rain rates 2.5 mm h^{-1}.

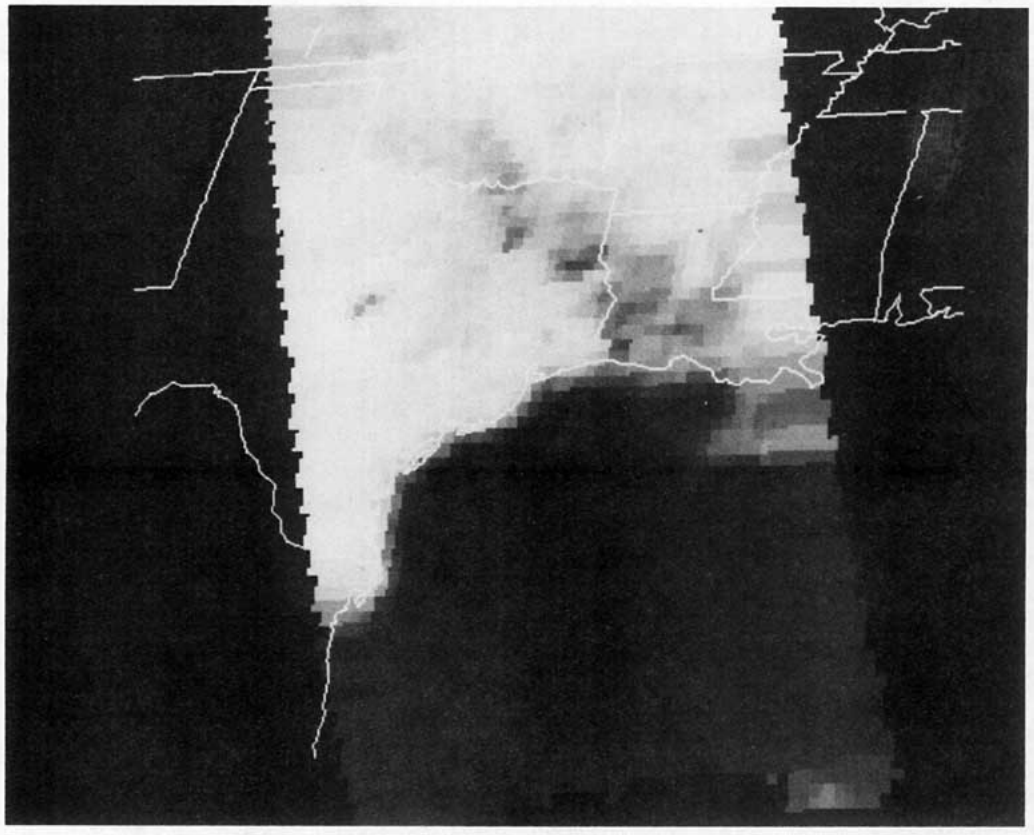

FIG. 4. The SMMR vertically polarized 37.0 GHz image of the similar area observed in Fig. 2 at the approximate same time. (See text.)

emissivity and T_s the surface thermodynamic temperature. The emissivity variation over land is due to the change in the dielectric constant of emitting surface and the biomass. A wet land surface has a larger dielectric constant and, therefore, a lower emissivity. Over water, the emissivity variation is mainly affected by ocean surface roughness. The emissivity varies from 0.40 over water to ~0.90 over dry land. Within the intervening atmosphere, the SMMR T_B is mainly affected by molecular oxygen, atmospheric moisture and cloud liquid water. The greater effect is due to enhanced absorption by liquid water, particularly large droplets with radii > 1 mm. In raining clouds where drops are larger than the wavelength, emittance becomes less and scattering greater than for drops smaller than the wavelength. Ice found in cirrus clouds is not a significant factor in the SMMR frequency range.

Thus, the warm vertically polarized 37 GHz T_Bs of the rain-free dry land areas in these SMMR images where the thermodynamic temperatures are greater than 15°C will appear light in shade while the lower T_B of the rain-free ocean areas will appear dark. Within rain areas observed by the WSR-57 radar over the Gulf of Mexico associated with the squall line, the enhanced emission of the radiation by the rain drops causes the T_Bs to be warmer (therefore, lighter in shade) than the T_B of the ocean background. Over land the opposite is true. Due to greater backscattering from larger raindrops, the T_Bs are relatively lower than those of the land background.

However, when the land surfaces are wet this contrast is greatly diminished since the T_Bs are lower due to the decreased emissivity of the background. As mentioned in Section 1, the lack of contrast can also be caused by the combination of the sensor's IFOV not being filled and the small dynamic range in T_B as a function of rain rate.

4. Statistical analysis

Elementary statistics of the sampled SMMR 37.0, 18.0, and 10.7 GHz data from the warm surface background cases are shown in Tables 2, 3 and 4. For each category the tables give sample size, the mean and standard deviation of the horizontally and vertically polarized T_B, and the correlation between T_H and T_V. The SMMR 37.0, 18.0, and 10.7 GHz data for the warm surface cases are also shown as scatter plots in Figs. 5, 6 and 7. In these figures the C rep-

TABLE 2. Elementary statistics of sampled 37 GHz data: Surface temperature ≥ 15°C.

	Rain area		Dry ground		Wet soil	
Sample size N	71		69		29	
	T_{HR}	T_{VR}	T_{HD}	T_{VD}	T_{HW}	T_{VW}
Mean	234	256	254	275	234	258
Mean brightness temperature difference	22		21		24	
Standard deviation d	7.9	7.7	3.2	2.8	6.7	7.6
Sample correlation coefficient between T_H and T_V ρ	0.96		0.97		0.88	

TABLE 4. Elementary statistics of sampled 10 GHz data: Surface temperature ≥ 15°C.

	Rain area		Dry ground		Wet soil	
Sample size N	71		69		29	
	T_{HR}	T_{VR}	T_{HD}	T_{VD}	T_{HW}	T_{VW}
Mean	248	254	260	268	229	244
Mean brightness temperature difference	6		8		15	
Standard deviation d	9.5	5.3	7.3	5.7	6.8	5.1
Sample correlation coefficient between T_H and T_V ρ	0.86		0.65		0.44	

resents the mean of the population and each frequency concentration ellipse encompasses 68% (one standard deviation) of the data within the population. The ellipses reveal the extent of scattering of the data from each population, the correlation between the dual polarization T_Bs (T_H and T_V) within each population (the higher the correlation, the larger the eccentricity of the ellipse) and the extent of overlap among the populations. The lines drawn in the figures are the Fisher (1938) linear discriminant lines which separate the rain over land areas (S_R), the dry land surface (S_D), and the wet land surface (S_W) populations represented by the T_B pairs (T_H, T_V) for each SMMR frequency.

It can be seen for the warm surface cases from Tables 2, 3, and 4 and Figs. 5, 6, and 7 that the average T_Bs for the rain areas over land are colder than those from dry land surface areas in all frequencies. However, they are warmer than the wet land surfaces for the 18.0 and 10.7 GHz SMMR channels. Also it is seen that the 37 GHz channel has the largest overlap of data between wet land surfaces and rain to an even greater extent than found in EMSR-6 data (Rodgers *et al.*, 1979). The reason for this overlap is that sometimes in sampling rainfall over land, the total upwelling radiance received by the radiometer contains a direct surface contribution. This may occur when the IFOV of the SMMR measurement is partially filled with moderate to heavy rain, or when it is completely filled with rain too light to attenuate the upwelling surface radiance. However, because of the larger dynamic range in T_H for the lower SMMR frequency channels, the overlap for 18.0 and 10.7 GHz T_B's became less even though their IFOV are larger. Again from Tables 2, 3 and 4, it is observed that the difference between the mean horizontally and vertically polarized T_Bs from rain areas over land (wet ground) becomes progressively smaller (larger) at low microwave frequencies. Although the difference is not as great as would be expected because of the mixed field of view problem, the ability to separate rain from wet land surface should improve, using the polarization differences in T_Bs at the lower frequencies. If, however, the polarization

TABLE 3. Elementary statistics of sampled 18 GHz data: Surface temperature ≥ 15°C.

	Rain area		Dry ground		Wet soil	
Sample size N	271		69		29	
	T_{HR}	T_{VR}	T_{HD}	T_{VD}	T_{HW}	T_{VW}
Mean	252	257	264	269	241	251
Mean brightness temperature difference	5		5		10	
Standard deviation d	4.6	3.7	4.2	2.6	7.1	5.2
Sample correlation coefficient between T_H and T_V: ρ	0.59		0.66		0.80	

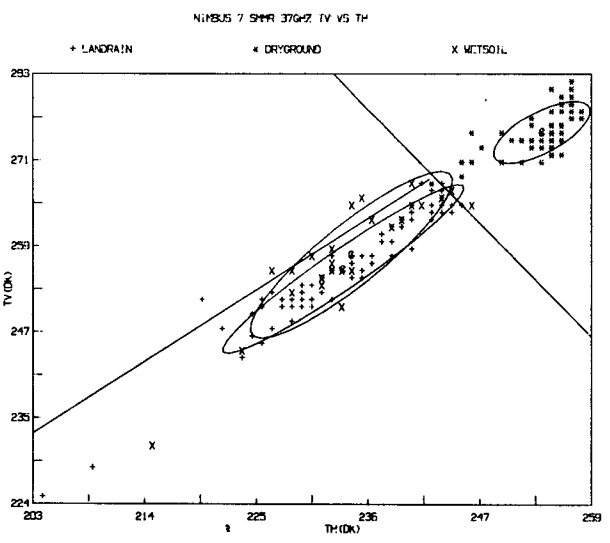

FIG. 5. Vertically polarized versus horizontally polarized SMMR 37.0 GHz T_B for each sampled category (rainfall over land, and wet and dry land surfaces). (See text.)

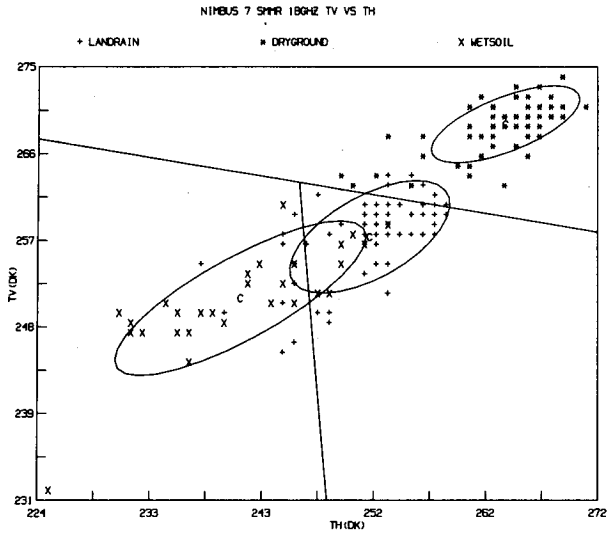

FIG. 6. As in Fig. 5, except for the SMMR 18.0 T_B.

differences, at the lower frequencies are not large enough to separate rain from wet land surfaces, misclassification of rain could be found in cloudy regions. Consider for instance, a cloudy case where the 18.0 GHz IFOV contains equal contributions from wet and dry land surface. The average horizontal and vertical T_B can easily fall within the standard deviation ellipse for the rainfall area and thereby be classified as rain. Therefore, misclassifications between rain and wet land surface using the lower frequency channel will depend on whether the rainfall is heavy and extensive enough to fill the radiometer IFOV.

In order to verify whether the three populations were statistically distinguishable from one another for the three SMMR channels, a variance ratio F test, in terms of Hotelling's T^2 and Mahalanobis' D^2 (Kshirsagar, 1972), was performed to determine the significance of the differences between the means of any two classes. It should be recalled that Mahalanobis' D^2 and Hotelling's T^2 between any two populations are measures of the separability of the two populations. The larger the values of D^2 and T^2, the greater the separability.

Tables 5, 6 and 7 display D^2 and T^2 as well as the computed and table (critical) value of F for the SMMR 37.0, 18.0, and 10.7 GHz channel data, respectively. All classes in each frequency except the 37.0 GHz wet ground and rain classes are well separated since computed values for any two populations of each frequency, except the values corresponding to 37.0 GHz rain and wet ground data of D^2 and T^2 are large. Similarly, because the observed value of F is much higher for each pair than the critical (table) value of F at 1%, the difference between the means of any two classes, except 37.0 GHz wet land and rain class mean difference, is statistically significant and the chances of any two of these means calculating is 1 in 100.

Elementary statistics of the sampled 37.0, 18.0 and 10.7 GHz data were also computed for the cold surface background cases. However, a decrease in surface thermodynamic temperature results in a decrease in T_B from dry ground and consequently, the contrast between dry land surfaces and rain over land will decrease at all frequencies. An examination of the 37.0, 18.0 and 10.7 GHz channels for the cold cases (surface thermodynamic temperatures < 15°C), substantiated this effect. As was demonstrated with the ESMR-6 data (Rodgers *et al.*, 1979) for cases in which thermodynamic temperatures were between 5 and 15°C, there was also considerable overlap of the SMMR 37.0 GHz data among the three populations (figures and tables not shown). This overlap was also observed in the SMMR 18.0 and 10.7 GHz channels. Thus, in the cases where the surface thermodynamic temperatures are <15°C the lower frequency channel did not help in distinguishing the three populations.

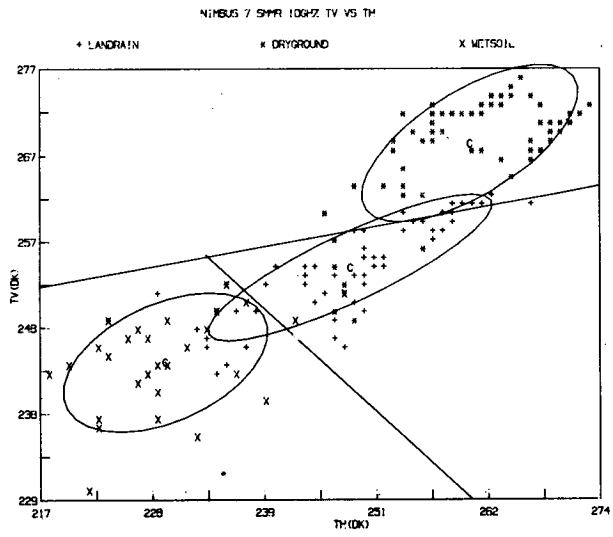

FIG. 7. As in Fig. 5, except for the SMMR 10.7 T_B.

TABLE 5. Significance between means (F test) SMMR 37 channel.

Between the means of	Mahalanobis distance squared D^2	Hotelling's T^2	Observed variance ratio F	Table value of F at 1%
Rain and dry	10	379	188	3.94
Dry and wet	12	261	129	4.00
Rain and wet	0.163	3.3	1.6	3.99

TABLE 6. Significance between means (F Test) SMMR 18 GHz channel.

Between the means of	Mahalanobis distance squared D^2	Hotelling's T^2	Observed variance ratio F	Table value of F at 1%
Rain and dry	12.67	443.38	220.08	3.94
Dry and wet	18.62	380.29	118.16	4.00
Rain and wet	3.33	68.66	33.98	3.99

5. Classification algorithm

Since most of the populations for the three channels were found to be statistically distinguishable for only the warm surface case, the Fisher linear discriminant classifier (Fisher, 1938) was considered with the purpose of developing a classification algorithm to detect and delineate rainfall over land from dry and wet land surfaces where thermodynamic temperatures were $\geq 15°C$, using the SMMR 37.0, 18.0, and 10.7 GHz data.

The purpose of the Fisher linear discriminant classifier is to determine a plane

$$Y = b_0 + b_1 T_H + b_2 T_V \tag{1}$$

which separates two given classes as widely as possible, given the variation of Y within the classes. The desired plane is the one for which b_1 and b_2 are determined by maximizing the function

$$G(b_1, b_2) = \frac{(\bar{Y}_1 - \bar{Y}_2)}{\sum_{i=1}^{2} \sum_{j=1}^{N_i} (Y_{ij} - \bar{Y}_i)^2}, \tag{2}$$

where $\bar{Y}_1$ and $\bar{Y}_2$ are the means of Y for the two classes and Y_{ij} is the jth value of Y in the ith class. The constant b_0 is determined so that the discriminant line

$$b_0 + b_1 T_H + b_2 T_V = 0 \tag{3}$$

defines the line of separation between the classes. Employing the data for each class and frequency, the following equations of the discriminant lines are determined:

$$L_{RD37} = 9.520 - 0.0215T_H - 0.016T_V = 0, \tag{4}$$

$$L_{RW37} = 1.823 + 0.029T_H - 0.033T_V = 0, \tag{5}$$

$$L_{RD18} = 17.455 - 0.011T_H - 0.056T_V = 0, \tag{6}$$

$$L_{RW18} = 10.6457 - 0.040T_H - 0.003T_V = 0, \tag{7}$$

$$L_{RD10} = -11.55 - 0.012T_H + 0.056T_V = 0, \tag{8}$$

$$L_{RW10} = 8.334 - 0.017T_H - 0.017T_V = 0, \tag{9}$$

where R = rain areas, D = dry ground, and W = wet land. These lines separate the classes S_D, S_R and S_W for the SMMR 37.0, 18.0, and 10.7 GHz channels, as shown in Figs. 5, 6 and 7. Thus, in the Fisher algorithm, the pixel corresponding to a given vector (T_H, T_V) is designated rain over ground, dry ground, or wet soil, respectively, depending on which of the following inequalities are satisfied:

I. 37 GHz Case:

$$\left.\begin{aligned} L_{RD37}(T_H, T_V) &< 0 \\ L_{RW37}(T_H, T_V) &< 0 \end{aligned}\right\}, \tag{10}$$

$$L_{RD37}(T_H, T_V) > 0, \tag{11}$$

$$\left.\begin{aligned} L_{RW37}(T_H, T_V) &> 0 \\ L_{RD37}(T_H, T_V) &< 0 \end{aligned}\right\}; \tag{12}$$

II. 18 GHz Case:

$$\left.\begin{aligned} L_{RD18}(T_H, T_V) &> 0 \\ L_{RW18}(T_H, T_V) &< 0 \end{aligned}\right\}, \tag{13}$$

$$L_{RD18}(T_H, T_V) < 0, \tag{14}$$

$$\left.\begin{aligned} L_{RW18}(T_H, T_V) &> 0 \\ L_{RD18}(T_H, T_V) &> 0 \end{aligned}\right\}; \tag{15}$$

III. 10 GHz Case:

$$\left.\begin{aligned} L_{RD10}(T_H, T_V) &< 0 \\ L_{RW10}(T_H, T_V) &< 0 \end{aligned}\right\}, \tag{16}$$

$$L_{RD10}(T_H, T_V) > 0, \tag{17}$$

$$\left.\begin{aligned} L_{RW10}(T_H, T_V) &> 0 \\ L_{RD10}(T_H, T_V) &< 0 \end{aligned}\right\}. \tag{18}$$

Obviously, ambiguity will result if any of these strict inequalities become equalities. Test on independent data are described in Section 7.

TABLE 7. Significance between means (F Test) SMMR 10 GHz channel.

Between the means of	Mahalanobis distance squared D^2	Hotelling's T^2	Observed variance ratio F	Table value of F at 1%
Rain and dry	6.48	227.09	112.72	3.94
Dry and wet	24.38	497.87	246.33	4.00
Rain and wet	5.46	111.29	55.07	3.99

6. Error analysis

An error estimate was made in order to evaluate quantitatively the performance of the Fisher classification algorithm for the three channels. The error

rates were computed according to the asymptotic formulas given by Okamoto (1963). From the results seen in Tables 8, 9 and 10, it is clear that the chance of incorrectly classifying wet land surfaces or dry land surfaces as rainfall over land is 51% using the 37.0 GHz channels. However, using the lower frequencies, the errors are greatly reduced (i.e. 23 and 24% for the 18.0 and 10.7 GHz channels, respectively). But when a given SMMR 18.0 or 10.7 GHz pixel is classified as raining area and each of the eight contiguous pixels that cluster around it is also classified as rainfall over land, then the chance of misclassification of that central pixel is reduced to approximately 7.7×10^{-6}% assuming each pixel is independently classified.

7. Algorithm evaluation

To qualitatively verify the performance of the Fisher classification algorithm, a case not previously sampled was tested. This case consisted of a synoptic-scale rain pattern over the southeastern United States associated with Hurricane Bob (at approximately 1700 GMT on 11 July 1979) which was observed by the SMMR. The surface thermodynamic, temperatures were >15°C. Figs. 8, 9 and 10 show the Centreville, Alabama, WSR-57 radar PPI image (white areas delineate rain rates > 2.5 mm h^{-1}), hourly rainfall amounts (mm) for the period from 1600 to 1700 GMT, and the storm's cloud top temperatures as measured from GOES-1 VISSR (cloud top temperature enhanced according to the scale mentioned in Section 3), respectively. The approximate times of the radar PPI and GOES-1 infrared measurements were within 5 min of the SMMR pass.

The results of the Fisher classification algorithm are seen in Figs. 11, 12 and 13, which show the location of the pixels (noted by dots) classified as rainfall over land using the 37.0, 18.0, and 10.7 GHz SMMR channel, respectively. The two lines encompassing the dots are the outer boundaries of the SMMR swath (i.e., ±50° of nadir).

It can be seen from Fig. 11 that the 37 GHz T_Bs are doing a surprisingly good job in differentiating the main rainfall patterns delineated by the WSR-57 radar PPI image (Fig. 8). For example, the large rain area in central and northern Alabama and eastern Mississippi, the rain band through southeastern Alabama and northwestern Florida, and the rain area in southern Tennessee, only observed by the Nashville, Tennessee (not shown) and ground recording stations (Fig. 9), were very well delineated by the 37 GHz channel.

However, there are areas in which the 37 GHz channel depicted rain where rain was not observed. These areas included extreme western Tennessee and Kentucky and southeastern Indiana and parts of western Illinois and eastern Missouri. With exception of Illinois and Missouri, the majority of these areas were cloudy with cloud top $T_{BB} < 270$ (see Fig. 10). The misclassification in the majority of these areas was caused by rivers, lakes and adjacent wet ground, such as the Mississippi River in southern Illinois and Lakes Barkley and Kentucky in western Kentucky. The reason for the misclassification in the other areas is also probably caused by wet land surfaces.

Examining the Fisher algorithm developed from the 18.0 and 10.7 GHz SMMR T_Bs (Figs. 12 and 13, respectively), one notes that very few pixels are classified as rain as compared to the algorithm developed from the 37 GHz data. This is because the lower frequency SMMR channels are less sensitive to rain (see Fig. 1). However, if the rain rates are high enough and fill the sensor's IFOV, the chances of misclassification of rain over land have been shown theoretically and observationally to be less than with the 37.0 GHz channel due to the large dynamic range in T_H for increasing rain rates.

From comparison of the Fisher algorithms developed from the 18.0 and 10.7 GHz SMMR T_Bs (Figs. 12 and 13, respectively) with the Centreville, Alabama, WSR-57 radar PPI image (Fig. 8), it appears that the majority of the pixels classified as rain are located in areas of rainfall depicted by the radar. Further, when the Fisher algorithm is compared with the hourly rainfall amounts between 1600 and 1700 GMT (Fig. 9) it also appears that the majority of the stations recording rainfall amounts greater than 1 mm during the hour are located within the cluster of

TABLE 8. Probabilities of misclassification: Theoretical computation SMMR 37 GHz channel (Average accuracy: 62%).

Classified	Rain	Dry	Wet
Rain	49	5	46
Dry	5	91	4
Wet	51	4	45

TABLE 9. Probabilities of misclassification: Theoretical computation SMMR 18 GHz channel (Average accuracy: 83%).

Classified	Rain	Dry	Wet
Rain	77	4	19
Dry	4	94	2
Wet	19	2	79

TABLE 10. Probabilities of misclassification: Theoretical computation SMMR 10 GHz channel (Average accuracy: 83%).

Classified	Rain	Dry	Wet
Rain	76	11	13
Dry	11	88	1
Wet	13	1	86

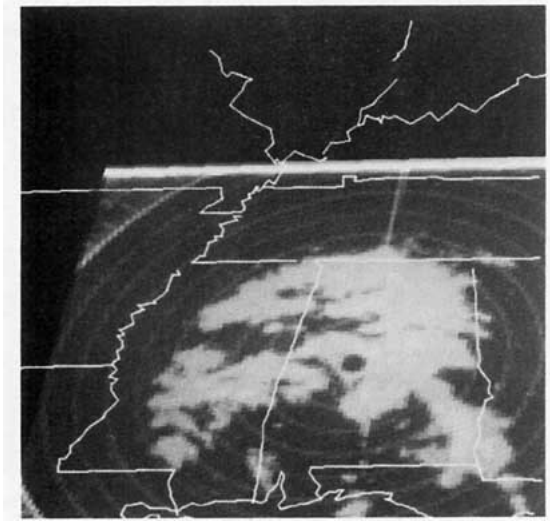

FIG. 8. The PPI image from the Centreville, Alabama SWR-57 radar at 1700 GMT on 11 July 1979. White areas represent rain rates 2.5 mm h^{-1}.

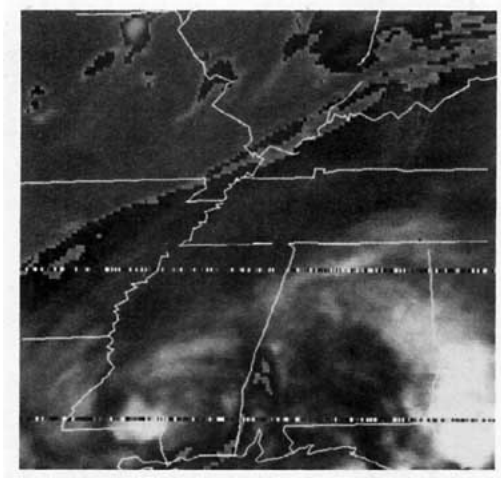

FIG. 10. The GOES-1 infrared image of tropical cyclone Bob observed at 1700 GMT 11 July 1979.

pixels that have been classified as rain in both channels. Heavy rain amounts measured by the ground stations in southeastern Mississippi were not classified as rain, since these pixels were near the edge of the SMMR swath. The pixels classified as rain areas in northern Georgia, western North Carolina and eastern Tennessee had rainfall rates less than 1 mm h^{-1} during the hour, according to the reporting stations. However, because of the orography in this area, these recorded rainfall amounts may not be representative of the rainfall rates that would be observed by SMMR.

The major discrepancy was with the algorithm developed with the 18.0 GHz data. The misclassified pixels were located in western Kentucky and northern Tennessee; this again may be caused by the wet land surfaces associated with the Mississippi River and Lakes Barkley and Kentucky. However, it can be seen in Fig. 13 that the algorithm developed from the SMMR 10.7 GHz T_B did not misclassify these pixels. This indicates that if the rainfall rates are heavy enough and fill the sensors IFOV, the 10.7 GHz channel would be the best of the three channels to differentiate rainfall from wet ground.

8. Conclusions

A statistical analysis was performed on the Nimbus-7 SMMR dual polarized 37.0, 18.0, and 10.7 GHz data for the purpose of assessing whether the 18.0 and 10.7 GHz channels could reduce the ambiguities found in the use of the 37.0 GHz radiometer data for differentiating rainfall areas from wet land surfaces. Results from the F test of the data showed

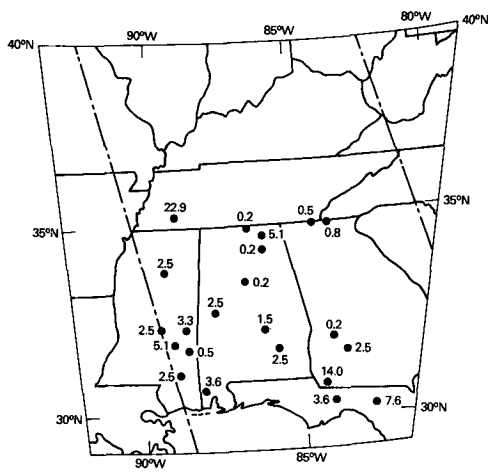

FIG. 9. Rainfall amounts in mm for the period 1600–1700 (GMT) 11 July 1979.

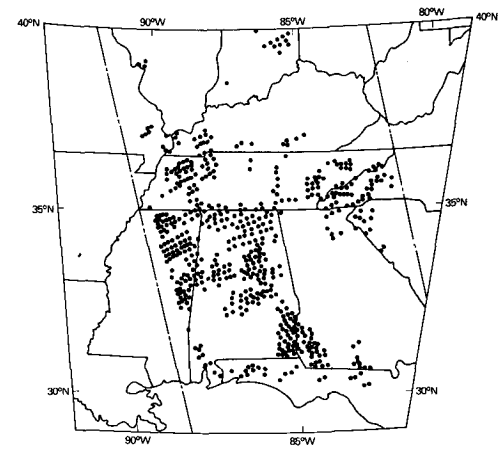

FIG. 11. Pixels (located by dots) classified as rain from the Fisher classification algorithm using the SMMR 37.0 GHz T_Bs.

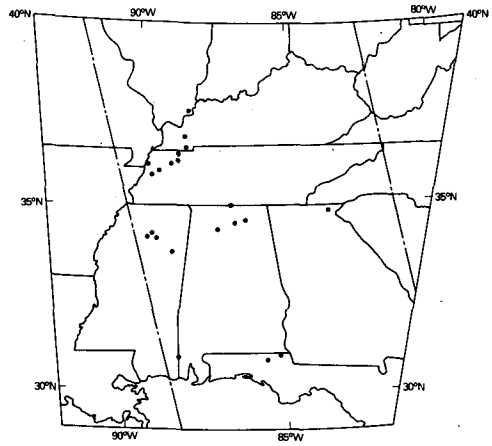

FIG. 12. As in Fig. 11 except the SMMR 18.0 GHz T_Bs.

that none of the SMMR channels could differentiate rain from wet or dry land when surface thermodynamic temperatures were <15°C. However, when the surface thermodynamic temperatures were ≥15°C, the F test indicated the probability that the mean vectors of any two populations being identical was less than 0.01 except for the rain over land and wet ground class observed with the SMMR 37 GHz channel. An error analysis of the SMMR data for the warm land surface cases revealed that the 37.0 GHz channel could correctly classify only rain or wet land from dry land, whereas the lower frequency SMMR channels could accurately classify rain from both dry and wet land surfaces, provided that the rainfall rates were high enough and sufficiently filled the sensor's IFOV so that the T_H was affected. An independent testing of the Fisher classification algorithms developed for each of the three SMMR channels further substantiated these findings. For example, there were areas misclassified as rain by the 37 GHz channel, but correctly classified by the lower frequency SMMR channels.

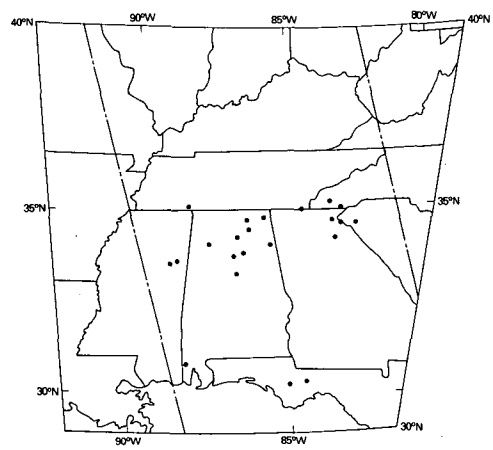

FIG. 13. As in Fig. 11 except the SMMR 10.7 GHz T_Bs.

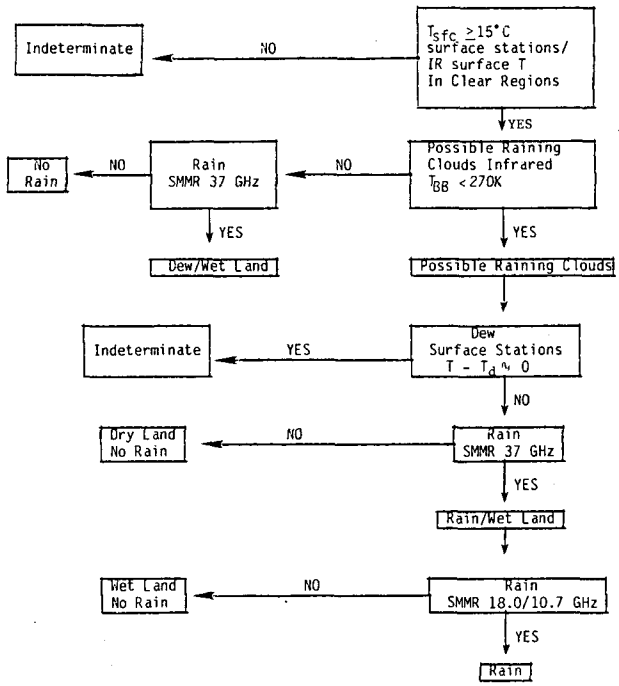

FIG. 14. Flow diagram suggesting a satellite technique for delineation of rainfall over land, using infrared and passive microwave data.

Thus, it appears that the lower frequency channels will better differentiate rain over dry or wet land surfaces. However, because the lower frequency SMMR channels are less sensitive to rain and have a larger IFOV, areas of light rain or rainfall occurring over small areas would not be observed. As observed in the independent test case, the 37 GHz channel did surprisingly well in delineating rain when compared to the radar in the cloudy areas whose cloud top T_{BB} was <270 K, even though there were areas of misclassification. Therefore, the study suggests that the ability to observe rainfall over land decreases with decreasing SMMR frequency. However, if rain is observed at these lower frequencies, the degree of confidence increases in delineating rainfall over land.

In light of the results of this study and the ESMR-6 study (Rodgers *et al.*, 1979), an improved rainfall-over-land detection technique could be developed by two different methods, utilizing both satellite infrared and multifrequency dual polarized passive microwave data. The first would utilize a more sophisticated statistical technique such as the Bayesian classification. The learning base would include the horizontally and vertically polarized T_Bs from the three SMMR channels together with the infrared radiance. The technique would be similar to the ESMR-6 study (Rodgers, *et al.*, 1979), except that there would be a seven-dimensional analysis rather than a two-dimensional.

A second but less quantitative method would be the one indicated by the flow diagram in Fig. 14, as follows:

1) Determination of the surface thermodynamic temperatures could be obtained from either surface meteorological data or from satellite infrared data in cloud free areas;

2) In areas where $T_{sfc} \geqslant 15°C$, the presence of possible raining clouds could be detected, again using satellite infrared data. Shenk *et al.* (1976) suggested that clouds that are probably producing rain have cloud top $T_{BB} < 270$ K;

3) To eliminate the problem of misclassification caused by dew at night when using the passive microwave data (Rodgers *et al.*, 1979), the dew point depression obtained from the surface stations would be examined, if available. However, the chances of dew occurring under cloudy conditions at night is less likely than during cloud free periods. A classification of rain by the 37 GHz SMMR data in clear regions at night would indicate either wet land or dew. If dew was indicated in the cloudy regions, the passive microwave data would not be able to differentiate rain from dew;

4) In the cloudy regions where cloud top T_{BB} are less than 270 K, the SMMR 37 GHz data would be used to differentiate rainfall and wet land from dry land;

5) Within these areas delineated as rain and/or wet land by the SMMR 37.0 GHz channels, the 18.0 and 10.7 GHz channels would be used to improve the degree of confidence that rain was being observed by the 37.0 GHz channel.

REFERENCES

Born, M., and E. Wolf, 1975: *Principles of Optics.* Pergamon Press, 182 pp.

Fisher, R. A., 1938: The statistical utilization of multiple measurements. *Ann. Eugenics,* **8,** 276–386.

Gloerson, P., and F. T. Barath, 1977: A scanning multichannel microwave radiometer for Nimbus-6 and Seasat-A. *IEEE J. Oceanic Eng.,* **OE-2,** 172–178.

——, and L. Hardis, 1978: The scanning multichannel microwave radiometer (SMMR) experiment. *Nimbus-7 User's Guide.* NASA Goddard Space Flight Center, 213–245.

Kshirsagar, A. M., 1972: *Multivariate analysis.* Marcel Dekker, 534 pp.

Negri, A. J., and R. F. Adler, 1981: Relation of satellite-based thunderstorm intensity to radar-estimated rainfall. *J. Appl. Meteor.,* **20,** 282–300.

Okamoto, M., 1963: An asymptotic expansion for the distribution of the linear discriminant function. *Ann. Math. Statist.,* **34,** 1286–1301.

Rodgers, E. B., H. Siddalingaiah, A. T. C. Chang and T. Wilheit, 1979: A statistical technique for determining rainfall over land employing Nimbus-6 ESMR measurements. *J. Appl. Meteor.,* **18,** 978–991.

Savage, R. C., and J. A. Weinman, 1975: Preliminary calculations of the upwelling radiance from rain clouds at 37.0 and 19.35 GHz. *Bull. Amer. Meteor. Soc.,* **56,** 1272–1274.

——, P. J. Guetter and J. A. Weinman, 1976: The observation of rain clouds over land in Nimbus-6 electrically scanned microwave and radiometer (ESMR-6) data. *Preprints 7th Conf. Aerospace and Aeronautical Meteorology and Symp. on Remote Sensing from Satellite,* Melbourne, Amer. Meteor. Soc., 131–136.

Shenk, W. E., R. J. Holub and R. A. Neff, 1976: A multispectral cloud type identification method developed for tropical ocean areas with Nimbus-3 MRIR measurements. *Mon. Wea. Rev.,* **104,** 284–291.

Weinman, J. A., and P. J. Guetter, 1977: Determination of rainfall distribution from microwave radiation measured by the Nimbus-6 ESMR. *J. Appl. Meteor.,* **16,** 437–442.

Wilheit, T. T., A. T. C. Chang, M. S. V. Rao, E. B. Rodgers and J. S. Theon, 1977: A satellite technique for quantitatively mapping rainfall rates over the oceans. *J. Appl. Meteor.,* **16,** 551–560.